Proc. of Urban Cultural Heritage Disaster Mitigation, Vol.2 (October 2008)

Numerical simulation of slope failure for mitigation of rainfall induced slope disaster of an important cultural heritage

Ha H. Bui [1], Kazunari Sako [1], Tomoaki Satomi [2], Ryoichi Fukagawa [3]

[1] Postdoctoral Fellow, Research Organization of Science & Engineering, Ritsumeikan University, Japan
[2] Graduate Student, Graduate School of Science & Engineering, Ritsumeikan University, Japan
[3] Professor, Department of Civil Engineering, Ritsumeikan University, Japan
(1-1-1 Noji-Higashi, Kusatsu, Shiga 525-8577, Japan)

The slope disaster prevention system, which is monitoring a slope located behind an important cultural heritage in Higashiyama-ward in Kyoto, has been developed in our research group to mitigate slope disaster due to heavy rainfall. In this system, the stability of a slope is evaluated by analyzing field measuring data, experimental models and numerical simulation results. In term of numerical simulations, unsaturated-saturated seepage behaviors have been investigated by finite element method, while slope stability analysis has been evaluated by limit equilibrium methods. To enhance the numerical models for the slope disaster prevention system, there is a need to implement a numerical method that can predict maximum displacement of soil after a slope failure, and possibility of occurrence of multi-stages slope failure during heavy rainfall. In this paper, an attempt is make to address the above requirements via simulating the progressive slope failure induced by rapid increase in water table level, which caused by heavy rainfall. Herein, the SPH framework for solving large deformation and failure flows of geomaterials [1] is adopted where soil was modeled using an elasto-plastic constitutive model. Several smoothed particle slope failure simulations are presented to investigate failure mechanism under different conditions. It is argued the SPH method is a needful implementation for the slope disaster prevention system to mitigate slope disaster due to heavy rainfall.

Key words: SPH (Smoothed particle hydrodynamics), slope failure, slope disaster mitigation, cultural heritage.

1. Introduction

Rainfall, especially heavy storms, has caused many landslides and slope failures. Such rain-induced landslides and slopes failures have posed serious threats and caused severe damage to many such countries as Japan, Hong Kong, Brazil, etc., over the years. As a result, studies on slope stability and slope failure under rainfall are attracting increasing attention in many countries especially in Japan. It has been reported that the landslide or slope failure under heavy rainfall condition was mainly caused by the rise in ground water level, and the increase in pore-water pressure or the decrease in matrix suction of unsaturated soil. Both the increase in pore-water pressure and the decrease in matrix suction cause the decrease in the shear strength of soil, which possibility leads to the occurrences of slope failure. Therefore, studies of saturated-unsaturated soil behaviors are of importance in evaluation of slope stability under heavy rainfall condition. On the other hand, our recent research, conducted at Fukagawa Lab. in Ritsumeikan University, is focusing on the development of a slope disaster prevention system where field measurement data, experimental modeling and numerical simulations are combined together to evaluate stability of a slope, which is located behind an important cultural heritage in Higashiyama-ward in Kyoto, during heavy rainfall. In the experimental study of slope failure due to heavy rainfall, it is noticed that the slope failure was caused by the erosion at the toe of the slope. It seems that the rise in ground water level speeds the seepage flow downstream to the toe of the slope. As a result, failure (boiling/erosion) occurs at the toe of the slope and then triggering the slope collapse. Furthermore, multi-stages failure process was often observed in such slope failure during a long heavy rainfall condition. To have an insight about the above failure mechanisms under heavy rainfall condition, there is a need to develop a numerical method which can be applied to simulate gross discontinuous failures.

In the field of computational geomechanics, finite element method (FEM) has been found to be the most attracting method for investigating stability of a slope under heavy rainfall condition. This is because FEM can be employed either to solve unsaturated-saturated seepage flow equation or to model soil deformation. However, FEM often encounters severe problem of grid distortion when attempt to simulate large deformation and failure flow of soil, for example the toe slope failure mechanism or the multi-stages failure

process mentioned above. On the other hand, the smoothed particle hydrodynamics (SPH), proposed by Gingold & Monaghan (1977) and Lucy (1997), has been recently developed for solving large deformation and failure flow of geomaterials (Bui et al. 2007; 2008). The SPH method represents a powerful alternative approach for slope stability analysis and discontinuous slope failure simulation (Bui et al., 2009) which offers similar advantages to FEM. Furthermore, SPH provides physical insight into the failure mechanisms of the slope due to its capability to simulate gross discontinuous failure. In this paper, the above SPH framework is adopted in an attempt to simulate progressive failure of a slope induced by the rapid increase in water table level. For sake of simplicity, the rapid increase in water table level is modeled by step loading procedure rather than solving seepage flow equation, which is postponed to a near future publication. Three examples of smoothed particle slope failure are presented to investigate failure mechanism under different conditions, including low water table level, high water table level, and progressive increase in water table level. As for the slope with low water table level, failure is not occurred. To trigger slope collapse, the shear strength reduction method (Griffths et al., 1999) is applied, thereby providing change to validate the current SPH model with traditional methods such as finite element method or limit equilibrium method. This paper argued that the SPH method is more powerful alternative to the traditional methods especially in handling large deformation and progressive failure problems. Therefore, the current application of SPH is a needful implementation for the slope disaster prevention system, which is being developed at Fukagawa Lab in Ritsumeikan University to mitigate slope disaster for an important cultural heritage in Kyoto.

2. Motion equation of soil in the SPH framework

An equilibrium equation of a continuum media, such as soil, can be described using following equation,

$$\rho \ddot{u}i^{\alpha} = \nabla_{\beta}\sigma'^{\alpha\beta} + \rho g^{\alpha} \tag{1}$$

where α and β denote Cartesian components x, y, z with the Einstein convention applied to repeated indices; ρ is the density; u is the displacement; σ' is the effective stress tensor; and g is the acceleration due to gravity. In the SPH framework, the above partial differential equation can be approximated through the use of a kernel interpolation, leading to

$$\ddot{u}_i^{\alpha} = \sum_{j=1}^{N} m_j \left(\frac{\sigma_i'^{\alpha\beta}}{\rho_i^2} + \frac{\sigma_j'^{\alpha\beta}}{\rho_j^2} + \Pi_{ij}\delta^{\alpha\beta} \right) \frac{\partial W_{ij}}{\partial x^{\beta}} + g^{\alpha} \tag{2}$$

where i is the particle under consideration; N is the number of neighbouring particles, i.e. those in the support domain of particle i; m is the mass of particle; $\prod_{ij}$ is the artificial viscosity, which is employed to damp out unphysical stress fluctuation; and W_{ij} is the smoothing function, which is chosen to be the cubic spline function (Monaghan, 1985).

The completed artificial viscosity appeared in equation (2) can be defined using the formulation proposed by Monaghan (1983). Herein, only an effect term of this formulation is adopted,

$$\Pi_{ij} = \begin{cases} \dfrac{-\alpha_{\Pi} c_{ij} \phi_{ij}}{\rho_{ij}} & (\dot{u}_i - \dot{u}_j)\cdot(x_i - x_j) < 0 \\ 0 & (\dot{u}_i - \dot{u}_j)\cdot(x_i - x_j) \geq 0 \end{cases} \tag{3}$$

in which

$$\phi_{ij} = \frac{h(\dot{u}_i - \dot{u}_j)\cdot(x_i - x_j)}{\left|x_i - x_j\right|^2 + 0.01h^2}, \qquad c_{ij} = \frac{c_i + c_j}{2}, \qquad \rho_{ij} = \frac{\rho_i + \rho_j}{2} \tag{4}$$

where α_{Π} is a constant parameter which is set to be 0.1; h is the smoothing length; and c is the sound speed, which should be chosen as the maximum value in soil (Bui et al., 2008).

As discussed by Bui et al. (2008), SPH encounters the so-called "tensile instability" problem when applied to cohesive soil. To remove this problem, Bui et al. (2008) have proposed to use an artificial stress term and proved the effectiveness of this approach. Accordingly, equation (2) is modified to

$$\ddot{u}_i^{\alpha} = \sum_{j=1}^{N} m_j \left(\frac{\sigma_i'^{\alpha\beta}}{\rho_i^2} + \frac{\sigma_j'^{\alpha\beta}}{\rho_j^2} + F_{ij}^{n} R_{ij}^{\alpha\beta} + \Pi_{ij}\delta^{\alpha\beta} \right) \frac{\partial W_{ij}}{\partial x^{\beta}} + g^{\alpha} \tag{5}$$

where

$$F_{ij}^{n} R_{ij}^{\alpha\beta} = \left[\frac{W_{ij}}{W(d_o, h)} \right]^n (R_i^{\alpha\beta} + R_j^{\alpha\beta}) \tag{6}$$

where n is a parameter; d_0 is the initial distance between particles; h is the smoothing length, which specified the non-zero region of the smoothing function; and R_{ij} is obtained as follows. For each particle the effective stress tensor $\sigma'^{\alpha\beta}$ is diagonalised. Then an artificial stress term is evaluated for any of the diagonal components $\overline{\sigma}'^{\alpha\beta}$ which are positive,

$$\overline{R}_i^{\gamma\gamma} = -\varepsilon_0 \frac{\overline{\sigma}_i'^{\gamma\gamma}}{\rho_i^2} \tag{7}$$

where ε_0 is a small parameter ranging from 0 to 1. The artificial stress in the original coordinates system R_{ij} is then calculated by reversing coordinates transformation.

Gray et al. (2001) derived optimal values from the dispersion analyses, and suggested to use $\varepsilon_0 = 0.3$ and $n = 4$ when applied SPH to solid. However, Bui et al. (2008) showed that these selections can not remove the tensile instability problem found when simulating cohesive soil. Instead, they suggested to use $\varepsilon_0 = 0.5$ and $n = 2.55$, and showed that these values have no effect on the modeled soil behaviour. In this paper, the same values are applied.

When considering the water table level or seepage flow behavior, the pore-water pressure (p_w) must be included in the momentum equation. According to Bui et al. (2009), the momentum equation (5) must be modified in the following way to include appropriate pore-water pressure,

$$\ddot{u}_i^{\alpha} = \sum_{j=1}^{N} m_j \left(\frac{\sigma_i'^{\alpha\beta}}{\rho_i^2} + \frac{\sigma_j'^{\alpha\beta}}{\rho_j^2} + F_{ij}^{n} R_{ij}^{\alpha\beta} + \Pi_{ij}\delta^{\alpha\beta} \right) \frac{\partial W_{ij}}{\partial x^{\beta}} + \sum_{j=1}^{N} \frac{m_j}{\rho_i \rho_j} (p_{wj} - p_{wi}) \frac{\partial W_{ij}}{\partial x^{\alpha}} + f^{\alpha} \tag{8}$$

This equation ensures that the gradient of a constant pore-water pressure field vanishes. On the other hand, numerical simulation will encounter instability problem, which leads to the failure of computation, if the gradient of the pore-water pressure is approximated using the same form as the gradient of the effective stress tensor. Furthermore, the above expression of pore-water pressure automatically imposes the dynamic boundary condition at the free surface. Finally, the above motion equation (8) can be solved directly using the standard Leapfrog algorithm if the effective stress tensor is known. Thus, it is necessary to derive constitutive equations for the effective stress tensor that are applicable in the SPH framework.

3. Soil constitutive modeling

According to the classical plasticity theory, the total strain-rate tensor of an elasto-plastic material $\dot{\varepsilon}$ can be decomposed into two parts: an elastic strain rate tensor $\dot{\varepsilon}_e$ and a plastic strain rate tensor $\dot{\varepsilon}_p$,

$$\dot{\varepsilon}^{\alpha\beta} = \dot{\varepsilon}_e^{\alpha\beta} + \dot{\varepsilon}_p^{\alpha\beta} \tag{9}$$

The elastic strain rate tensor $\dot{\varepsilon}_e^{\alpha\beta}$ is given by a generalized Hooke's law, i.e.,

$$\dot{\varepsilon}_e^{\alpha\beta} = \frac{\dot{s}^{\alpha\beta}}{2G} + \frac{1-2\upsilon}{E} \dot{\sigma}'^{m} \delta^{\alpha\beta} \tag{10}$$

where $s'^{\alpha\beta}$ is the deviatoric effective shear stress tensor; υ is Poisson's ratio; E is the elastic Young's modulus; G is the shear modulus and σ'^{m} is the mean effective stress.

The plastic strain rate tensor is calculated by the plastic flow rule, which is given by

$$\dot{\varepsilon}_p^{\alpha\beta} = \dot{\lambda} \frac{\partial g}{\partial \sigma'^{\alpha\beta}} \tag{11}$$

where $\dot{\lambda}$ is the rate of change of plastic multiplier, and g is the plastic potential function.

In the current study, the Drucker-Prager model with non-associated flow rule is applied to model the soil behavior. Accordingly, plastic deformation will occur only if the following yield criterion is satisfied,

$$f(I_1, J_2) = \sqrt{J_2} + \alpha_{\phi} I_1 - k_c = 0 \tag{12}$$

where I_1 and J_2 are, respectively, the first and second invariants of the stress tensor; α_{ϕ} and k_c are Drucker-Prager constants, which are calculated from the Coulomb material constants c (cohesion) and ϕ (internal friction). In plane strain, the Drucker-Prager's constants are computed by,

$$\alpha_\phi = \frac{\tan\phi}{\sqrt{9+12\tan^2\phi}} \quad \text{and} \quad k_c = \frac{3c}{\sqrt{9+12\tan^2\phi}} \tag{13}$$

For the non-associated plastic flow rule, the plastic potential function is given by,

$$g = 3I_1 \sin\psi + \sqrt{J_2} \tag{14}$$

Substituting equations (10), (11) into (9), and adopting the Jaumman stress rate for large deformation treatment, the stress-strain relation for the current soil model at particle *i* becomes,

$$\dot{\sigma}_i'^{\alpha\beta} = \sigma_i'^{\alpha\gamma}\dot{\omega}_i^{\beta\gamma} + \sigma_i'^{\gamma\beta}\dot{\omega}_i^{\alpha\gamma} + 2G_i\dot{e}_i^{\alpha\beta} + K_i\dot{\varepsilon}_i^{\gamma\gamma}\delta_i^{\alpha\beta} - \dot{\lambda}_i\left[9K_i\sin\psi_i\,\delta^{\alpha\beta} + (G/\sqrt{J_2})_i s_i'^{\alpha\beta}\right] \tag{15}$$

where $\dot{e}_i^{\alpha\beta} = \dot{\varepsilon}_i^{\alpha\beta} - \frac{1}{3}\dot{\varepsilon}_i^{\gamma\gamma}\delta^{\alpha\beta}$ is the deviatoric shear strain rate tensor; ψ is the dilatancy angle; $\dot{\lambda}_i$ is the rate of change of plastic multiplier, which in SPH is specified by,

$$\dot{\lambda}_i = \frac{3\alpha_\phi K\dot{\varepsilon}_i^{\gamma\gamma} + (G/\sqrt{J_2})_i s_i'^{\alpha\beta}\dot{\varepsilon}_i^{\alpha\beta}}{27\alpha_\phi K_i\sin\psi_i + G_i} \tag{16}$$

and $\dot{\varepsilon}_i^{\alpha\beta}$, $\dot{\omega}_i^{\alpha\beta}$ are the strain rate and spin rate tensors defined by,

$$\dot{\varepsilon}_i^{\alpha\beta} = \frac{1}{2}\left(\frac{\partial\dot{u}^\alpha}{\partial x^\beta} + \frac{\partial\dot{u}^\beta}{\partial x^\alpha}\right)_i \quad \text{and} \quad \dot{\omega}_i^{\alpha\beta} = \frac{1}{2}\left(\frac{\partial\dot{u}^\alpha}{\partial x^\beta} - \frac{\partial\dot{u}^\beta}{\partial x^\alpha}\right)_i \tag{17}$$

The above soil constitutive model requires three soil parameters, the cohesion coefficient (*c*), friction angle (ϕ) and elastic bulk modulus (*K*), which can be specified from a simple shear box test or triaxial test.

4. Problems description and boundary conditions

(1) Slope model and setting conditions

Fig.1 shows the slope model used for numerical investigation. This slope is assumed to be made of homogeneous soil with $E = 10^5$kN/m^2, $\upsilon = 0.3$, $\phi = 20^o$, c = 20.6kN/m^2, and $\gamma = 21$kN/m^3. Initially, the water table level is set at 10m high, and then it is enforced to increase by step loading, which is controlled by two parameters θ and *h*. The parameter θ controls the gradient of pore-water pressure downstream to the slope toe, while the parameter *h* controls the water level. Each parameter has a maximum value, for an instant $\theta_{max} = 15^o$ and $h_{max} = 6$m are employed in the current paper. When the loading starts, the water level under the slope (left side from the toe) is pushed up via θ and *h*, while the water level in the open slope foundation (right side from the toe) is kept constant. The loading is performed in 8s and simulation is carried out until the completion of slope collapse. In addition to the loading water table, two additional numerical simulations employed a constant water table are also performed to verify difference with the loading case as well as to validate the SPH framework. The first one is associated with the low water table level ($\theta_{min} = 0^o$ and $h_{min} = 0$m), while the second one is concerned with the high water table level ($\theta_{max} = 15^o$ and $h_{max} = 6$m).

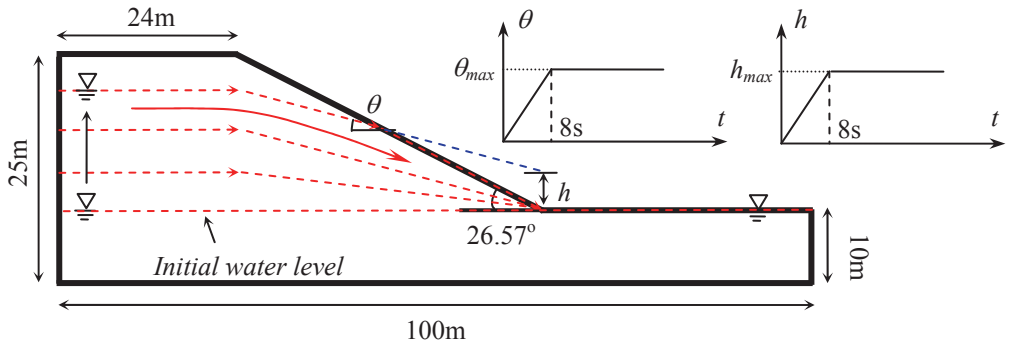

Fig.1. Slope model geometry and initial setting condition

(2) SPH boundary conditions

The boundary conditions consist of vertical rollers on the faces at the left and right ends and full fixity at the base of the slope foundation. In the SPH framework, the rollers are modeled using ghost particles, while the fix boundary condition is modeled using SPH boundary particles. For details description of such boundary conditions, we refer readers to the recent publication (Bui et al., 2008).

(3) Shear strength reduction method

The slope model shown in Fig.1 will not collapse if the water table level is set at a low level, i.e. $\theta_{min} = 0^o$ and $h_{min} = 0$m. In such case, to make comparison with other cases, in which the slope will collapse due to increase in the water table level, the shear reduction technique (Griffths et al., 1999) is adopted to trigger the slope collapse.

In the shear strength reduction technique, a series of numerical tests are performed with reduced shear strength parameters c^{trial} and ϕ^{trial} defined as follows,

$$c_{trial} = \frac{c}{FOS^{trial}} \qquad \text{and} \qquad \phi_{trial} = \boldsymbol{arctan}\left(\frac{\tan\phi}{FOS^{trial}}\right) \tag{20}$$

where c and ϕ are real shear strength parameters, and FOS^{trial} is the trial safety factor. Normally, initial FOS trial is set sufficiently low so that the system is stable. Then, the value of FOS^{trial} is increased gradually until the slope fails. The final value of FOS^{trial} that makes the slope fail is defined as the safety factor of the slope, which is identical to the one in limit equilibrium method.

5. Numerical applications and discussion

(1) Validation of SPH for slope failure simulation

In this section, mechanism of slope failure in the SPH framework is examined. Two numerical examples with a low water table level ($\theta_{min} = 0^o$ and $h_{min} = 0$m) and a high water table level ($\theta_{max} = 15^o$ and $h_{max} = 6$m) are performed and then comparing to the limit equilibrium method, i.e. Bishop, in term of safety factor (FOS) and critical slip surface.

Similar to FEM analysis of slope stability, a serial of SPH slopes are performed via shear strength reduction method in association with the convergent and unconvergent analyses (Bui et al., 2009) in order to find the minimum factor of safety (FOS) at which the slope is failure (unconvergent solution). This minimum factor of safety in SPH corresponds to the safety factor calculated by the limit equilibrium method. On the other hand, the critical slip surface can be automatically predicted via the contour plot of accumulated plastic shear strain. No additional assumptions are make in the current SPH model.

Fig.2 shows the SPH result for slope failure simulation, which corresponds to the unconvergent solution. Herein, the SPH method predicts $FOS = 1.38$ for the slope with ($\theta_{min} = 0^o$ and $h_{min} = 0$m) and $FOS = 0.93$ for the slope with ($\theta_{max} = 15^o$ and $h_{max} = 6$m). These results are in very close agreement with the limit equilibrium method, which gave $FOS = 1.37$ for the former case and $FOS = 0.91$ for the latter case.

Regarding the critical slip surface, Fig.2a shows the contour plot of accumulated plastic strain corresponding to unconvergent SPH solutions as compared to the circular slip surface obtained from the limit equilibrium method. It can be seen that SPH predicts very clear critical slip surface via thin layer of plastic strain localization, which is very difficult to model by FEM. Again, close agreements are obtained between

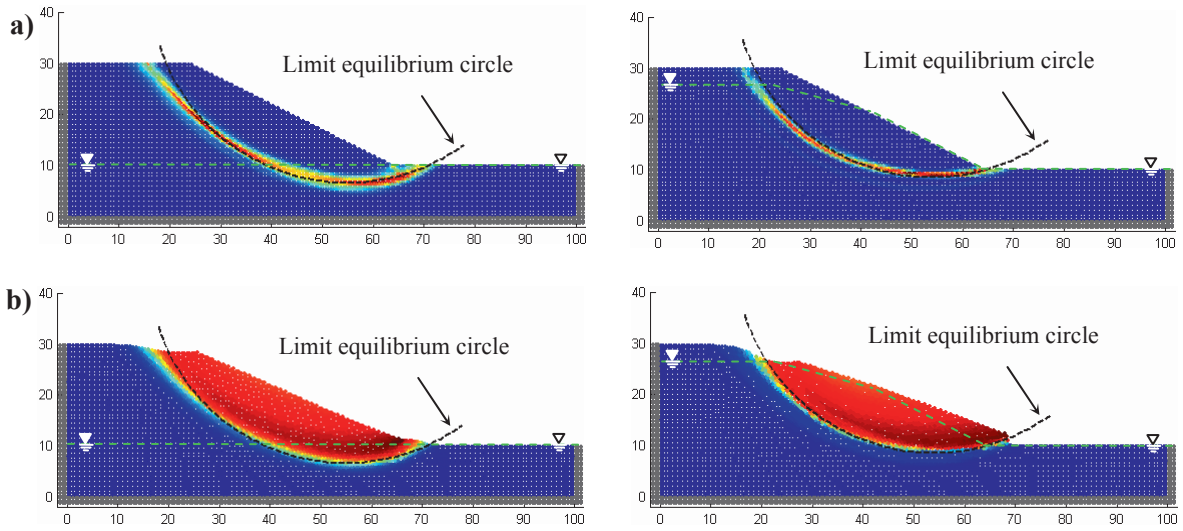

Fig.2. Slope failure simulation by SPH: (a) Contour plot of accumulated plastic shear strain; (b) Contour plot of total displacement at the final deformation. Color is auto adaptive.

SPH and limit equilibrium method. The slight difference between two methods can be explained by the assumption of circular slip surface employed in the limit equilibrium method. Furthermore, the toe failure mechanism is also observed in both cases with a deeper mechanism extending into the foundation layer for the case with lower water table level. It is noted that two slip surfaces were observed for the case with high water table, suggesting that multi-stage failure process may be simulated by SPH.

Fig.2b shows the final configuration of the slopes after collapse, via contour plot of total displacements. The result shows that gross discontinuities of the slope along the potential slip surface, which is unable to model by FEM, can be described very well by SPH. Numerical simulation can be performed as long as desired without encountering any problems. Furthermore, comparison between two cases shows that the failure zone is enlarged for the case with lower water table level. However, the lager maximum displacement was observed for the case with higher water table level.

(2) Progressive slope failure due to the increase in water table level

The above numerical illustrations of SPH for slope stability analysis and slope failure simulation show good agreement with the traditional approaches. Thus, the SPH method is extended to simulate progressive slope failure due to rapid increase in water table. Instead of solving seepage flow equation, the water table herein is risen by loading two parameters θ and h in 8s to reach their limits $\theta_{max} = 15^{o}$ and $h_{max} = 6$m. The change in pore-water pressure is then applied to the momentum equation, i.e. the second term in the right hand side of equation (8). A similar procedure will be employed when solving seepage flow equation for either saturated or unsaturated soil.

As for the water table, Fig.3a shows the typical development of hydrostatic pore-water pressure at the base of the slope foundation (left hand side from the crest of the slope) and corresponding pore-water distribution in the slope. Herein, distribution of pore-water pressure is divided into three sections: left hand side from the crest of the slope; middle between the crest and the toe of the slope; and right hand side from the slope toe. When θ and h were loaded, new straight line namely gradient line, which passed through a point located at ($x = 64$; $y = 10+h$) and having slope angle of $-\theta$, is formed. The pore-water pressure in the middle section was then calculated as the product between unit weight of water (γ_w) and the vertical elevation from a considering point to the gradient line or the slope surface. On the other hand, the pore-water pressure on the left hand side is calculated based on the vertical elevation from a considering point to the horizontal line, which passes through the intersection between the gradient line and the vertical line that goes through the crest of the slope.

Fig.3b shows the maximum total displacement with respect to time at the unconvergent SPH solutions in comparison among three cases, which are low water table, high water table and loading water table. It can be seen that without employing the step loading of water table, the slope failure failures immediately until reaching a new equilibrium possition. It is noted that the low water table slope was collapsed because of employing the shear strength reduction method. On the other hand, for the case of loading water table, the slope is stable in about 7s before collapsing. In term of the maximum total displacement, we noticed that the maximum total displacement was observed for the slope that employed the step loading in water table although the final water level is the same with the high water table slope. This difference may be explained

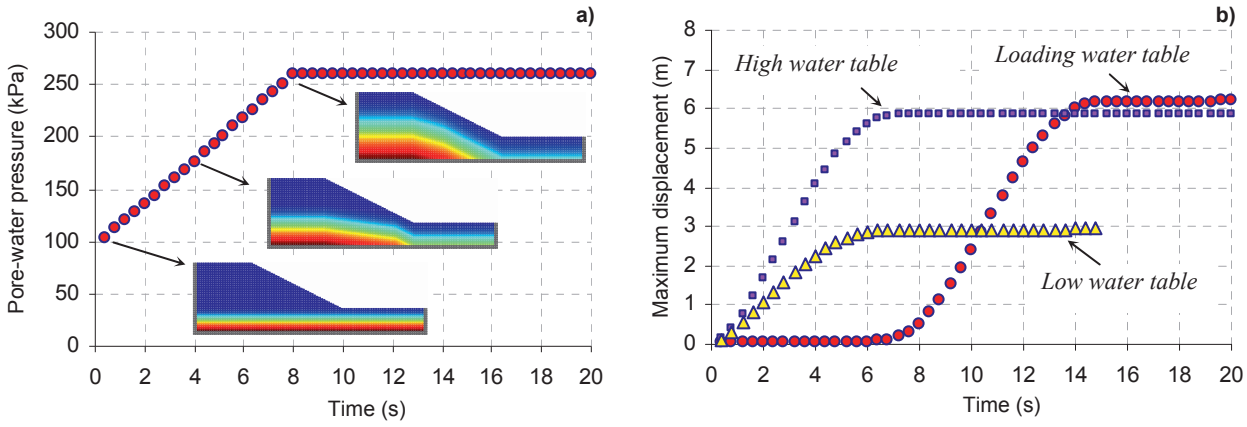

Fig.3. Distribution of pore-water at the base of the slope foundation (**a**) and maximum total displacement of soil at unconvergent SPH solution (**b**).

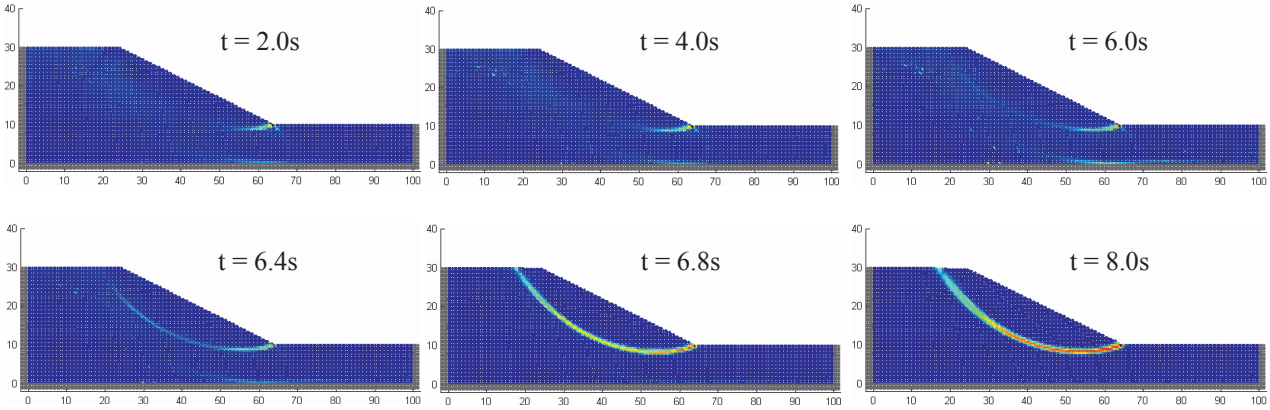

Fig.4. Formation of critical slip surface during the step loading of water table level

due to an inertial force, which is caused by rapidly increasing in pore-water pressure, applied on the sliding block during progressive failure.

Fig.4 shows the formation of critical slip surface via contour plot of accumulated plastic shear strain. From this figure, it can be seen that the failure process was initiated from the toe of slope and then propagating to the crest of the slope. The plastic shear strain developed very slowly at the beginning of the failure process as shown in the upper images, and then turned to develop rapidly until the total collapse of the slope as illustrated by the lower images. It should be noted that the step loading of water table level was also performed until t = 8s where the formation of critical slip surface was completed. We expected that by adopting the powerful SPH technique in handling large deformation and failure, the erosion at the toe of the slope can be simulated. However, because of the simplicity in solving seepage flow, and because the soil cohesion was kept constant in simulations, the current SPH model hasn't yet provided full explanation of the toe erosion process. On the other hand, the current SPH model provided the insight to the propagation of slope failure, which was initiated from the slope toe. We suggested that by carefully solving unsaturated-saturated seepage flow equation, and taking into account change of cohesion during rainfall, such erosion process can be reproduced by SPH. With this respect, we are working on this approach.

Fig.5 shows the failure process of the slope after collapse via contour plots of accumulated plastic shear strain and corresponding total displacements. Again, the gross discontinuous failure of the slope along the critical slip surface can be simulated very well by SPH, and numerical simulation can be performed as long as desired without encountering any problems. In comparison to the previous slopes, there is a slight difference, regarding the displacement of the crest of the sliding block, between the current slope and the slope that employed high water table level (θ_{max} = 15^o and h_{max} = 6m), however the critical slip surface is almost the same between two cases. Regarding the progressive failure, it is well-known that the slope failure due to heavy rainfall is often associated with multi-stages failure. Herein, only the first stage of slope failure was observed since the water table level in the current simulation was constrained. However, if we remove the constraint of the water table level, the multi-stages failure process of the current slope can be reproduced.

Fig.6 shows the second stage failure of the current slope obtained when the constraint of water table level was removed. Herein, only h is permitted to increase without limitation, while θ was kept at the same

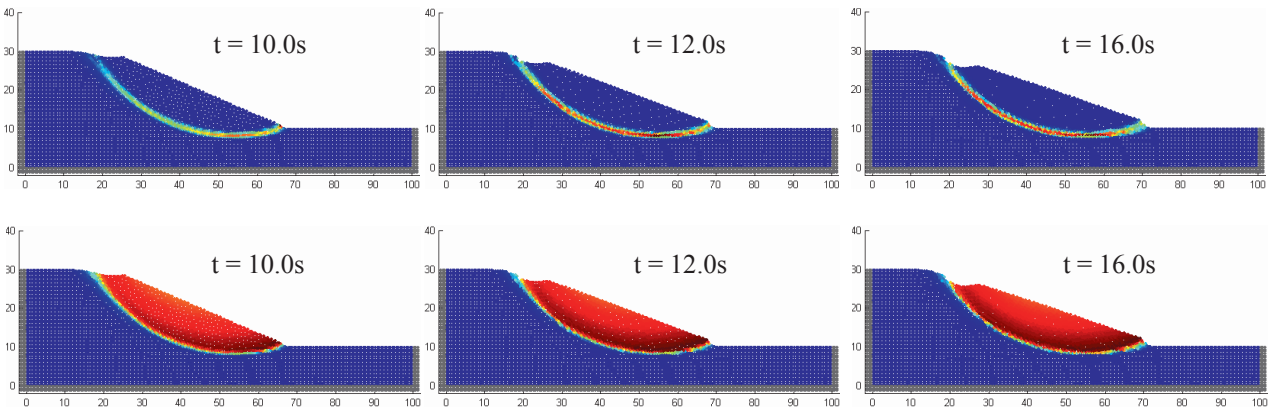

Fig.5. Failure mechanism of the slope due to the rapid increase in water table via contour plots of plastic shear strain (upper images) and total displacement (lower images)

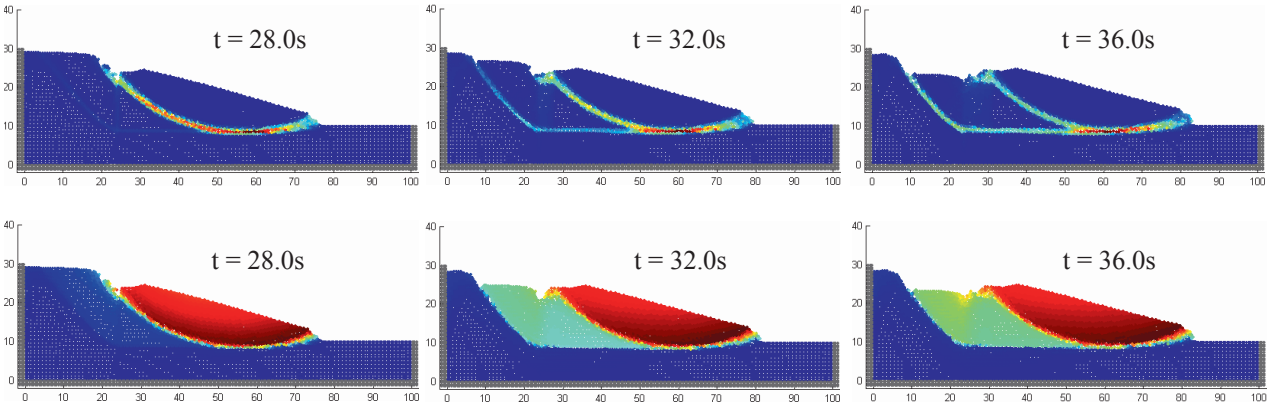

Fig.6. Multi-stage failure process (second stage failure) of the slope via contour plots of plastic shear strain (upper images) and total displacement (lower images)

limitation. Therefore, when the gradient line moves beyond the crest of the slope, the step loading of water table level only affects the left hand side section of the slope counting from the crest of the slope. As seen in Fig.5, the current slope reached a new stable position after the fist stage failure. However, because of the continuous increase in water table level, which may be caused by a long heavy rainfall in reality, the second failure stage occurred at the deeper section to the left as shown in Fig.6 via contour plots of shear plastic strain and total displacement. The process will be continued if the water table level is kept increasing. This is reality as compared to the well-known multi-stages slope failure at the Tokai-Hokuriku Expressway. From this simulation result, it confirmed that the SPH method is a powerful alternative for simulation of progressive slope failure. The authors suggest that by considering the unsaturated-saturated seepage flow and taking into account change in soil strength during heavy rainfall, more accurate progressive slope failure simulation can be predicted by SPH.

6. Concluding remarks

The smoothed particle method in conjunction with an elasto-plastic (Drucker-Prager) stress strain model has been shown to be a reliable and robust method for simulating the progressive slope failure due to rapid increasing in water table level, which is caused by heavy rainfall. One of the main advantages of SPH is that it can handle the gross discontinuous failure of soil, thereby applicable for simulating the multi-stages slope failure. Furthermore, using the proposed method, it is also possible to predict safety factor of a slope and maximum displacement of soil after a slope failure. These suggest that SPH is a needful implementation for the slope disaster prevention system, which is being developed at Fukagawa Lab. to mitigate slope disaster for an important cultural heritage located in Higashima-ward in Kyoto. The authors are encouraged by the current simulation results but recognized the need for further implementations of unsaturated-saturated seepage flow behavior to the current SPH framework. In the near future, the completed numerical model will be applied to the real slope in the concerning area.

References

1. Bui H. Ha, Fukagawa R., Sako K., Ohno S: Lagrangian mesh-free particles method (SPH) for large deformation and post-failure of geomaterial using elastic-plastic soil constitutive model, *Int. J. Numer. Anal. Meth. Geomech.*, Vol. 32(12):1537-1570, 2008.
2. Bui H. Ha, Sako K, Fukagawa R.: Slope stability analysis and slope failure simulation by SPH, *The 17th International Conference on Soil Mechanics and Geotechnical Engineering (ICSMGE)*, Egypt, Oct. 2009. (Accepted)
3. Bui H. Ha, Sako K, Fukagawa R.: Innovative solution for slope stability analysis and discontinuous slope failure simulation by elasto-plastic SPH, *Geotechnique*, (in preparation).
4. Gingold RA, Monaghan JJ. Smoothed particle hydrodynamics: Theory and application to non spherical stars. *Mon. Not. Roy. Astron. Soc.*, 181:375-389, 1977.
5. Gray JP, Monaghan JJ, Swift RP. SPH elastic dynamics. *Computer Methods in Applied Mechanics and Engineering,* 190:6641-6662, 2001.
6. Griffths DV, Lane PA. Slope stability analysis by finite elements. *Geotechnique*, 49(3):387-403, 1999.
7. Monaghan JJ, Lattanzio JC. A refined particle method for astrophysical problems. *Astronomic and Astrophysics*, 149:135, 1985.
8. Libersky LD, Petschek AG, Carney TC, Hipp JR, Allahdadi FA. High strain lagrangian hydrodynamics: A three dimensional SPH code for dynamic material response, *Journal of Computational Physics*, 109:67-75, 1993.
9. Lucy L. A numerical approach to testing the fission hypothesis. *Astronomical Journal*; 82:1013-1024, 1997.